https://doi.org/10.1016/j.apenergy.2019.03.091

Consistency Analysis of Polymer Electrolyte Membrane Fuel Cell Stack during Cold Start

Rui Lin[1*], Yike Zhu[1], Meng Ni[2], Zhenghua Jiang[1], Diming Lou[1*], Lihang Han[1], Di Zhong[1]

[1]School of Automotive Studies, Tongji University, Shanghai 201804, Shanghai, China

[2]Building Energy Research Group, Department of Building and Real Estate, The Hong Kong Polytechnic University, Hong Kong, PR China

Abstract

This paper investigates the cold start characteristic of the polymer electrolyte membrane fuel cell stack in the constant voltage startup mode. The stack is used in actual vehicle working conditions, so it is practical significance to study the cold start characteristics of the stack. The evolution of the temperature and current density distribution at different regions in the constant voltage mode of the stack are studied. Consistency analyzes from two dimensions, in-plane and through-plane are studied. Then, the performance degradation of the stack after the cold start is explored through the polarization curve and the voltage consistency.

The cold start characteristics and performance degradation mechanism of the stack are found. The stack has better cold start performance than that of the single cell, which can realize a rapid cold start at -15°C in 95s. Also, the performance of the single cell in the middle position is obviously better than that of the single cell on both sides. The internal behavior of each single cell during cold start process is different and the performance consistency is poor after the failed cold start. The performance degradation gradually decreases from the single cell near the inlet to the single cell far away from the inlet. This paper can provide direction for the optimization cold start strategy.

Keywords: PEMFC Stack; Cold start; Segmented cell technology; Consistency

1. Introduction

PEMFC has many advantages, such as no pollution, fast startup, high efficiency and so on [1,2]. Therefore, it is widely used in various fields[3]. Its subzero startup capability is one of the main constraints to its commercialization[4]. In the subzero environment, water produced by electrochemical reaction accumulated in the cell. When the accumulated water exceeded the maximum water saturation, the water would freeze[5]. The ice blocked the reactive sites in the catalytic layer, which in turn led to cold start failure. In order to overcome this

* Corresponding author: E-mail address: ruilin@tongji.edu.cn (R. Lin), loudiming@tongji.edu.cn (D.M. Lou)

problem, many experimental and numerical studies were conducted to investigate the cold start processes and improve the cold start ability of the single cell. Since the super-cooled water was present in cold starting fuel cell, liquid water management strategies might also be used to enhance cold start capability[6]. The addition of the microporous layer could effectively improve the cold start performance of the single cell [7]. The reason was that the microporous layer could improve the water management ability of the single cell. Yang et al. [8]investigated the effect of MPL's hydrophobicity on the output performance and ice/water distribution. Decreasing the MPL's hydrophobicity led to higher current density and helped to remove the super-cooled water, which in turn decreased the ice formation in catalyst layer. Xie et al. [9]investigated the effect of ionomer/carbon (I/C) ratio on PEMFC cold start. It was found that decreasing the I/C ratio could improve the membrane water absorption and reduce ice formation. The reaction core area moved to the side closer to the membrane with I/C ratio decreased. Huo et al. [10]studied the water transport behavior and phase transition mechanisms during the cold start process. The liquid water in the cathode catalytic layer tended to rise slowly and drop rapidly during the cold start process, indicating that the liquid water should freeze mostly. Ko et al. [11]developed a multiphase transient model to investigate key physical and transport phenomena during the cold start process. They found that the effect of startup temperature on the cold start performance of the fuel cell was significant. Huo et al. [12]investigated the cold start processes of proton exchange membrane (PEM) fuel cells with two different designs for cathode flow fields, metal foam and conventional parallel. They found that metal foam could enhance the normal and cold start performance of PEM fuel cell, because it had the high porosity, outstanding water storage ability and controllable thermal conductivity. Gas purge for eliminating water from gas diffusion layer, membrane and catalytic layer was important for PEMFC cold start, because it could improve cell durability and cold start performance[13]. Do not over-purge and ensure the minimum amount of water required for the proton conductivity of ionomer and membrane[14]. Knorr et al. [15]used methanol-water solution as antifreeze for polymer electrolyte membrane fuel cell at the single cell level. They discovered that the performance degradation was fully eliminated by the antifreeze. In addition, vacuum assisted drying could also replace gas purge[16]. Hishinuma et al. [17] found that under the condition of no external assistance, only cold start above -5 ℃ could success.

In general, the cold start modes included constant voltage, constant current and constant power mode[18]. Lin et al. [19] compared the cold start characteristics of the single cell by a constant voltage mode. It was found that the lower the starting voltage, the more rapid the cold start speed was. Amamou et al. [20] proposed to control the real-time operating current of the cell to achieve rapid cold start.

There were many simulation studies on the cold start of the stack. Chippar et al. [21]used a three-dimensional PEMFC cold start model to analyze the cold start characteristics of the single cells in the middle position and at both ends of the stack. The results show that the heat preservation of the end plate was the key to improve the temperature rise rate and the cold start performance of the stack. Luo et al. [22] had established a (PEMFC) stack model and found that the icing rate of the stack with more single cells was lower. The temperature and performance uniformity of the cells located in the middle position of the stack was better than that of the others[5,23]. Tang et al[24] developed a fuel cell stack model that could track the rate of ice formation in porous media. Zhan et al.[25] explored many auxiliary cold start methods for the stack, such as heating air, heating coolant, etc. These auxiliary measures could effectively improve the cold start performance of the stack, but would increase the cost of the system.

Freezing during low temperature startup was the main reason for the failed cold start process[26]. The repeated freezing / thawing cycle during startup process would damage the key components of the cell, which would lead to the deterioration of PEMFC performance and the decrease of durability[27]. The voltage decline of the single cell in different positions of the stack is different[28]. It was very important to find out the mechanism of cold start performance degradation of the stack and provide the direction for optimizing cold start strategy.

In-situ measurement was an important and effective method to study the distribution of reactants and local electrochemical reactions. The evolution of the current density and the temperature in each zone were investigated during cold start process by PCB technology[29,30]. The PCB was installed between the MEA and anode plate to collect current. The PCB technology could monitor the electrochemical reaction in different areas of the cell in real time so that the researchers could fully understand the performance of different regions. Kim et al. [31] studied the uniform distribution of clamping force in the flow field by segmented technology.

However, most of the cold start researches were mainly for single cells, and there were few reports on the research on the stack, which were mainly concentrated on simulation. Due to the idealization of boundary conditions and other conditions, the simulation results could not truly and reliably reflect the actual situation of the PEMFC cold start process. This paper used experimental methods that could more realistically reflect the internal behavior of the stack during the cold start process. The cold start characteristics of the stack were explored under different start-up temperatures and starting load modes. In order to understand the evolution of the current density distribution during the cold start process of the stack, this paper used the segmented cell technology. Consistency is analyzed from two dimensions. One was the different regions of the single cell(in-plane). The other was the different single cells in the stack(through-plane). The performance degradation of

the stack after the cold start was explored through the polarization curve and the voltage consistency. The general rules of successful or failed cold start at low temperature were obtained. This paper could provide direction for optimizing cold start strategy of the stack in the real applications.

2. Experiment system and control

Fig. 1 shows the structure of the stack. The experimental stack was composed of five single cells, and the effective active area of the single cell was 50 cm^2. The main parameters of the stack were summarized in Table 1. With printed circuit board technology, the current density and the temperature distributions in PEMFC could be measured through experimental methods[19,29,32]. The PCB was installed between the MEA and anode plate to collect current. The anode flow field on the PCB was the three-channel serpentine flow field, dividing the active area of the flow field into 49 segments as shown in Fig. 2[19]. Mark them with number 1-7 and alphabet A-G. A1 was the hydrogen outlet region. G7 was the hydrogen inlet region. The real-time acquisition (PCB) of the segmented current density and temperature was performed for the 1(#1), 3(#3), and 5(#5) single cells. The cell numbers #1, #2, #3, #4, and #5 described here all adopted the numbering method from the anode side to the cathode side of the stack. The following single cell numbering methods were in accordance with the above numbering rules.

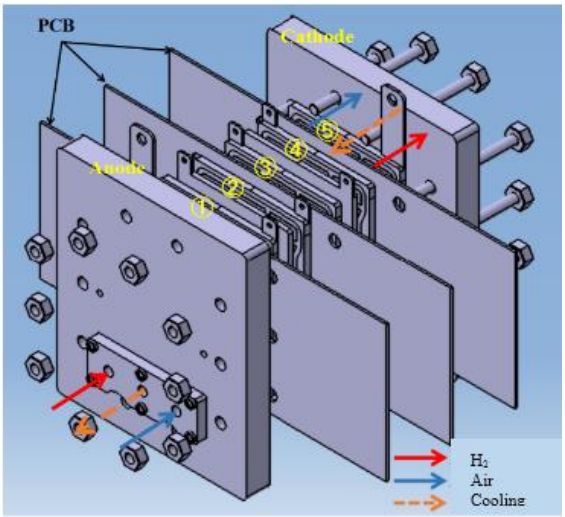

Fig. 1. The structure of the stack

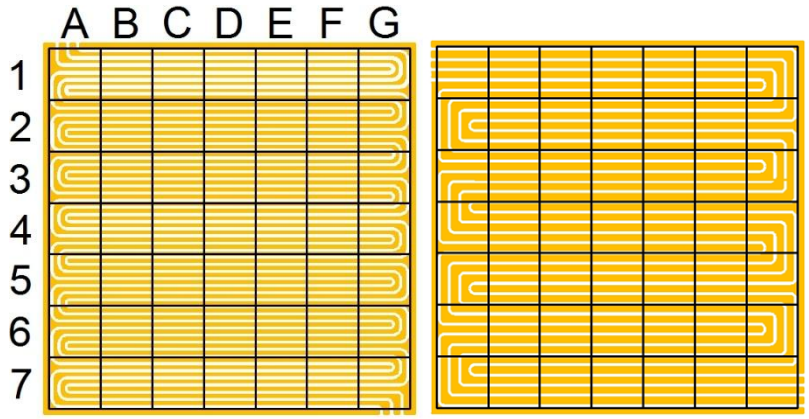

Fig. 2. The flow fields structure of the stack (left: the anode flow field segmented carved on the PCB; right: the cathode flow field)

Table 1 Summary of main parameters of the stack

Parameters	Value
Number of single cells	5
Series or parallel connection	series connection
MEA	Commercial MEA
Effective active area	50 cm^2
Flow field structure	anode：triple serpentine flow field cathode：fourth serpentine flow field
Channel width and height	1mm
Ridge width	0.4mm
Clamping method	bolt clamping（7.5 N·m）
Cooling method	water

The G60 fuel cell test system was used to control the backpressure, load, gas flow rate and humidity and other operating parameters. The environmental chamber which ranged from -40 to 150℃ was used to control start-up temperature to imitate subzero environment. The reaction gases went through a 3m long cooling pipe in the environmental chamber to ensure the temperature of the reaction gas entering the PEMFC was the same as the set temperature of the environmental chamber[19].

Experimental procedure:

(1) Activation. Before the cold start experiment, the stack needed to be activated. The hydrogen and air stoichiometry were 2 and 3, the stack temperature was 70 ℃, the back pressure was 0.6 bar and the relative humidity was 65%. The output voltage was controlled to be 0.6 V for the first 2 h and 0.4 V for the next 2 h. After activation, measure the polarization curve.

(2) Purging. The anode and cathode were purged by dry nitrogen. The purge flow for the anode/cathode were 3.5/5.0 L min^{-1}. The purge duration of the cold start experiment was 1h.

(3) Freezing. Place the stack in the environmental chamber and set the temperature of the environmental chamber to the start-up temperature (-5°C, -10°C, -15°C and -20°C). The stack freezing time was 4h.

(4) Cold start. The inlet flow of the anode/cathode was 2.5/5.0 L min^{-1}. The reaction gases were not humidified and didn't have a back pressure during the cold start process. After the start-up process, the stack needed to be activated before the next cold start experiment. Then measure the polarization curve of the stack.

The parameters to be investigated during the cold start process of the stack were shown in Table 2, including the starting temperature, starting load size. In order to ensure accuracy, every experiment was repeated for two times.

Table 2 The cold start parameters of the stack

Parameters	Value			
Temperature	-5℃	-10℃	-15℃	-20℃
Mode	Constant voltage	Constant voltage	Constant voltage	Constant voltage
	1.5V	1.5V	1.0V	0.5V
	2.0V	2.0V	1.5V	1.0V
	2.5V	2.5V	2.0V	/

3. Results and discussion

The achieved results from the stack cold start experiments were explored in this section. The first part of the analysis was related to the cold start characteristics of the stack in constant voltage mode and compared the difference between the cold start performance of the stack and the single cell. The second part of the analysis was the evolution of the temperature and current density distribution during cold start process of different single cells in the stack. The third part of the analysis dealt with the performance degradation of the stack by the cold start.

3.1. The cold start characteristics of the stack in the constant voltage mode

The effect of the starting voltages on the cold start performance of the stack at different temperatures was shown in Fig. 3. Choose the temperature of the single cell with the worst temperature rise characteristic in the stack as the stack temperature. Fig. 3 (a) and Fig. 3 (b) show that the stack had a nice cold start capability at -5 °C and -10 °C. The average current density firstly increased quickly because the membrane got hydrated by the super-cooled water and therefore the ohmic resistance reduced[19,33].

The stack could achieve a rapid cold start in 280s and 95s in Fig. 3(c) when cold start from -15°C at 1.5 V

and 1.0 V, respectively. Lin et al.[19] realized rapid cold start of the single cell in 170s (-10°C at 0.3 V), but the stack only needed 35s. In addition, the single cell all failed when cold start from -15 °C, but the stack could realize rapid cold start in 95s. The reason was that the stack had better heat preservation ability than that of the single cell[21]. Moreover, the cell with a good cold start performance in the stack might transfer heat to the cell with poor performance, and each cell would cooperate with others. Therefore, the stack had better cold start performance than that of the single cell[22].

However, the cold start from -20 °C all failed in Fig. 3(d).The water produced by the electrochemical reaction was rapidly frozen at the three-phase reaction interface in the early stage of the cold start at -20 °C [34]. The effective active area of the catalytic layer was gradually reduced, and the output current was decreased[26]. Finally, when the ice volume exceeded the ice storage capacity of the stack, which indicated that the catalyst layer and gas supply were completely blocked, current density became 0 A cm^{-2} and cold start failed[7,9,19]. Therefore, the lower the temperature, the more difficult the successful cold start was.

From the results of the successful cold start at -5°C, -10°C, and -15 °C, it could be found that the cold start speed could effectively increase by reducing the startup voltage. It could be seen from the equation (1) that reducing the starting voltage could increase the heat production power of the stack and improve the cold start performance when the open circuit voltage of the stack was constant[26,29,35].

$$P_{heat} = (E_0 - u_{stack}) \times i_{stack} \qquad (1)$$

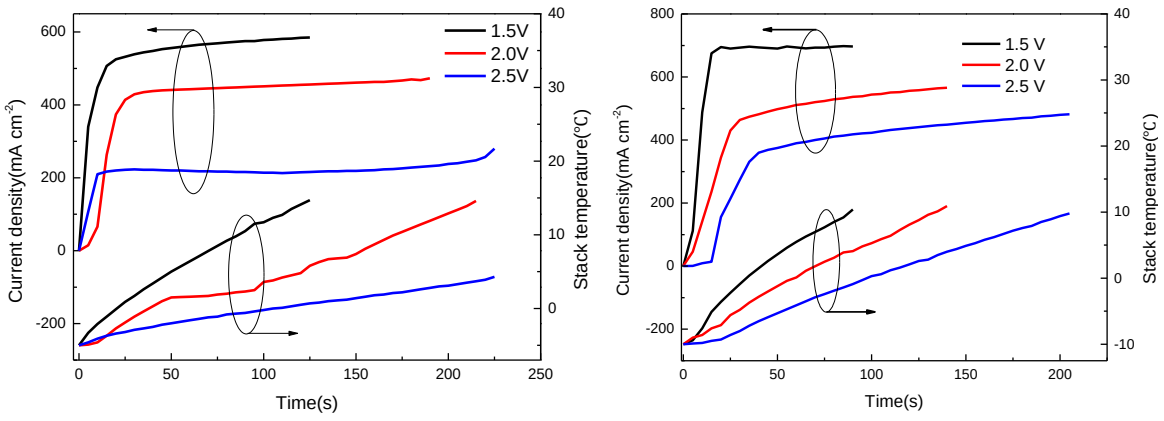

(a) -5°C (b) -10°C

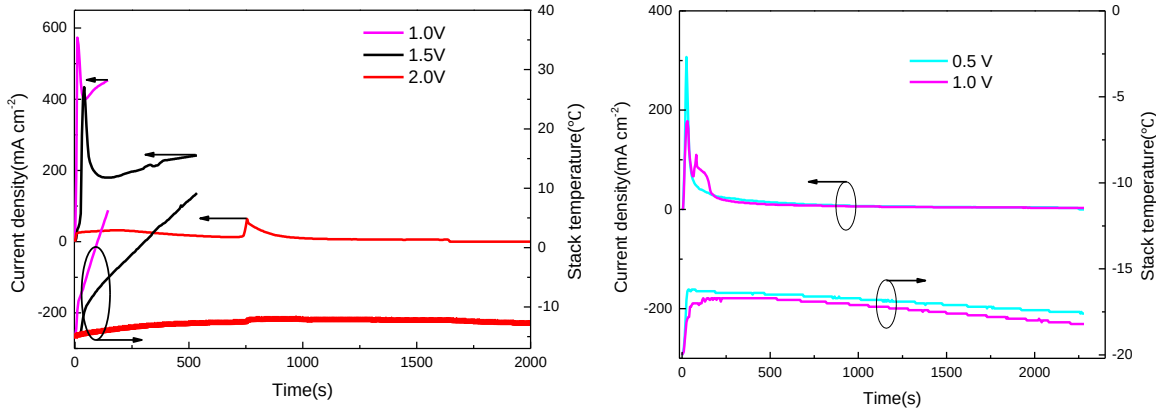

(c) -15°C (d) -20°C

Fig. 3. Effect of starting voltage on the cold start performance of the stack under different starting temperatures

Detailed cold start time under different load conditions was summarized in Table 3.

Table 3 Summary of the stack cold start time under different load conditions

Load/ temperature	0.5V	1.0V	1.5V	2.0V	2.5V
-5℃	/	/	30s	55s	85s
-10℃	/	/	35s	60s	100s
-15℃	/	95s	280s	failed	failed
-20℃	failed	failed	/	/	/

3.2. Evolution of the single cells temperature and current density distribution during cold start process

This section detailed the internal behavior of cells during cold start process.

3.2.1. Evolution of the single cells temperature during cold start process

Fig. 4 shows the evolution of the single cells (#1, #3, #5) temperature when cold start process from -5°C, -10°C, -15°C and -20°C. The temperature rising during the cold start process of each single cell was inconsistency. The temperature rising of the #3 single cell located in the middle position was the fastest [5,23]. It took 30s and 25s for the #1 and the #5 single cell to reach 0°C when cold start from -5°C at 1.5V, while the #3 single cell only needed 20s. It took 95s and 80s for the #1 and #5 single cell when cold start from -15°C at 1.0 V, but the #3 single needed 55s, respectively. When cold start from -20°C at 0.5V, although the final cells all failed, the maximum temperature of the #3 single cell was -15.5°C. It was obviously higher than that of the others. During the cold start process, the #3 single cell contributed the most heat. The reason was that the cell in the middle position might have a relatively small surface area in direct contact with the environment compared with the single cell located at both ends, resulting in less heat dissipation[21]. Therefore, the insulation effect of the middle position single cell

was the best. The #1 single cell had the worst cold start performance. On the one hand, the #1 single cell directly exchanged heat with the environment. On the other hand, the inlet gases had a great disturbance to the temperature of the #1 single cell.

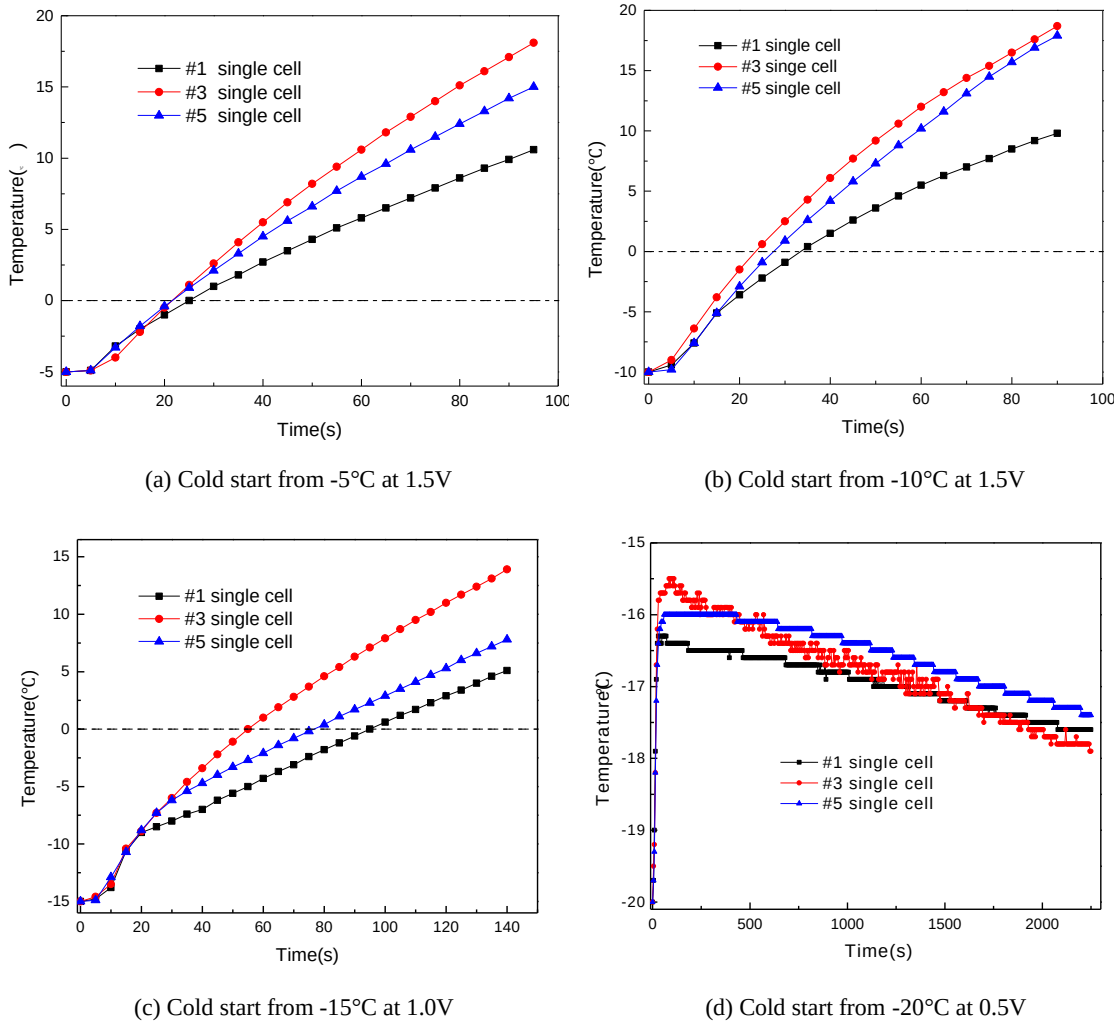

(a) Cold start from -5°C at 1.5V

(b) Cold start from -10°C at 1.5V

(c) Cold start from -15°C at 1.0V

(d) Cold start from -20°C at 0.5V

Fig. 4. Evolution of the single cells (#1, #3 and #5) temperature

3.2.2. Evolution of the current density distribution of the stack during successful cold start process

Fig. 5 shows the evolution of the current density distribution of the single cells (#1, #3 and #5) for the successful cold start from -5°C, -10°C and -15°C at constant voltage start mode. It shows the inconsistency in current density variation in the different cells and the different regions of the same cell. The current density appeared firstly near the inlet region (G7), and then diffused along the flow channel to the middle region and the outlet region in Fig. 5[32]. The current generation process was accompanied by the production of water and heat[36]. When the heat production rate was faster than that of the freezing rate, the cell continued to warm up and finally realized the successful cold start[26]. The stack had fine cold start ability at -5°C and -10°C because the

uniformity of the cells was well as shown in Fig. 5(a) and Fig. 5(b). Moreover, the effective area of the MEA had small ice coverage[26]. However, the uniformity of the cells decreased when cold start from -15°C because there was much heat loss near the surround of the plate[37]. In general, the distribution of high current density mainly concentrated in the middle region and therefore the middle region had a major contribution to the heating of the stack.

Moreover, Fig. 5(a) shows that local starvation (gas flow back) occurred in the # 5 single cells at 25s. This was due to an insufficient supply of reactive gas[38]. Starvation produced extra energy. If we could not supply enough protons and electrons, other substances would be corroded[39]. For example, water electrolysis produced protons, carbon corrosion, catalyst corrosion and so on[7]. Therefore, the heating rate of the # 5 single cell was higher than that of the # 1 single cell. However, the performance and the durability of the fuel cell would decrease due to the degradation of the catalyst layer and growth of the Pt particles[40]. So, we could increase the inlet flow to improve the cold start performance of the stack and realize rapid cold start[41,42].

Fig.6 shows that the current density response of the single cells different zones of the single cells (#1, #3 and #5) during the successful cold start at -15 °C. The current density appeared firstly at G7 (hydrogen inlet) region. It was the core region of electrochemical reaction within 5s. The D4 region current density was larger than that of the average current density because it had the lowest heat loss and sufficient reaction gases. The middle (D4) region had the highest current density and therefore played a leading role during the cold start process[19,29,32,43]. The current density of the outlet region was lower than that of the average current density. Therefore, the heat generation in the middle (D4) region had a major contribution to raise the temperature of the stack.

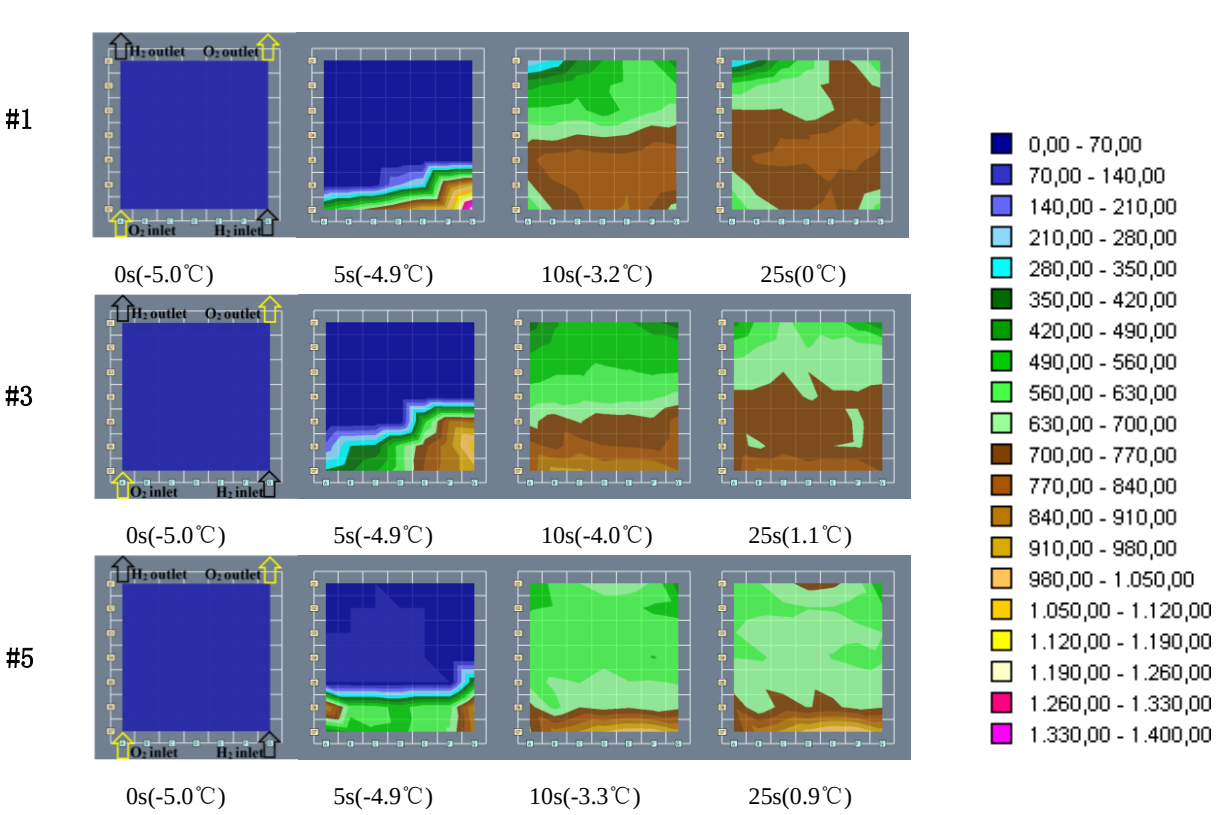

(a) Cold start from -5°C at 1.5V

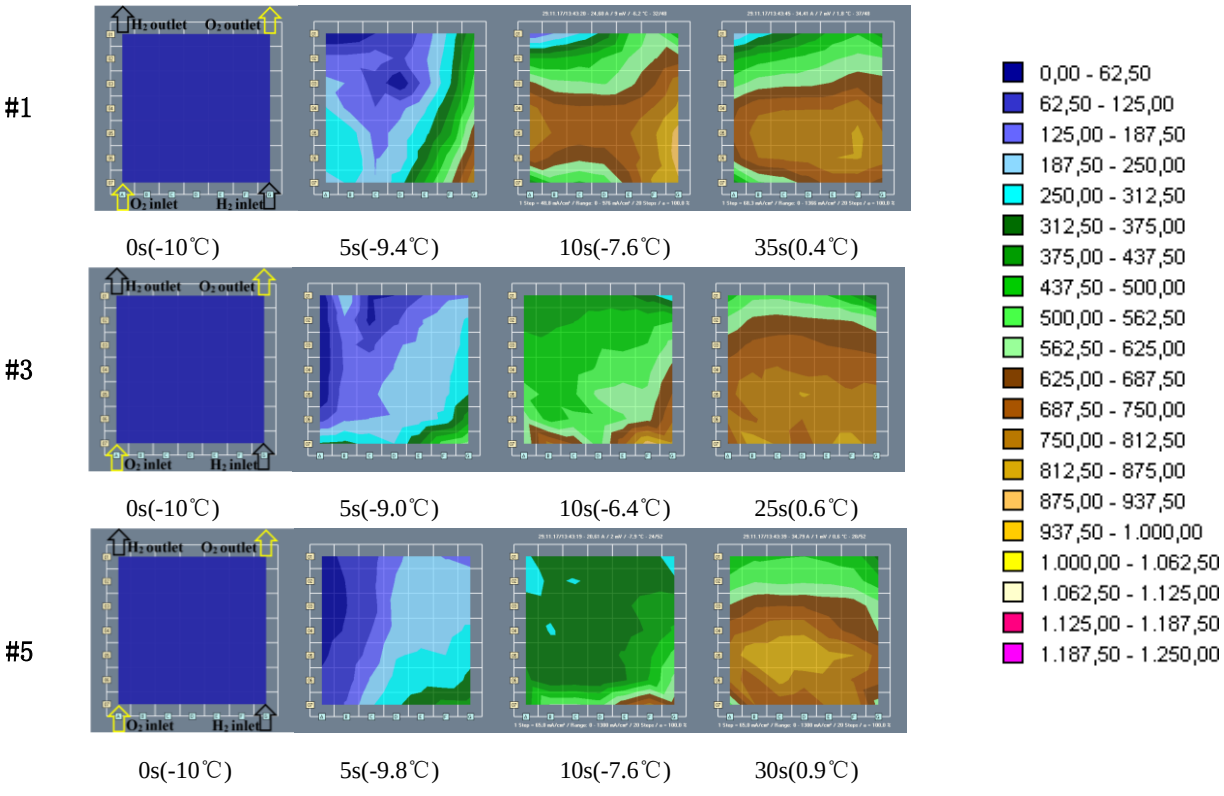

(b) Cold start from -10°C at 1.5V

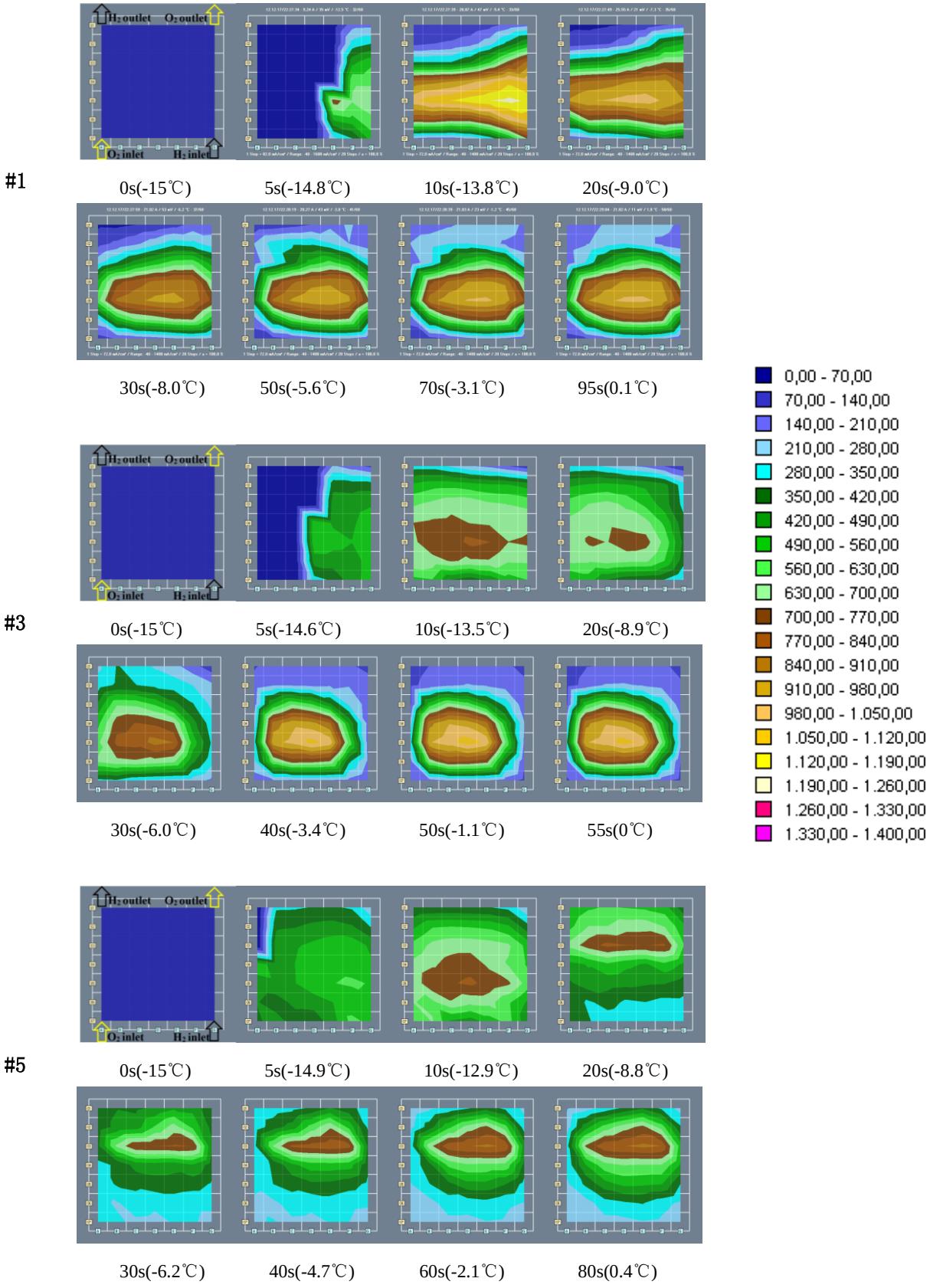

(c) Cold start from -15°C at 1.0V

Fig. 5. Evolution of current density distribution of the single cells (#1, #3 and #5) for the successful cold start from -5°C, -10°C and -15 °C at constant voltage start mode

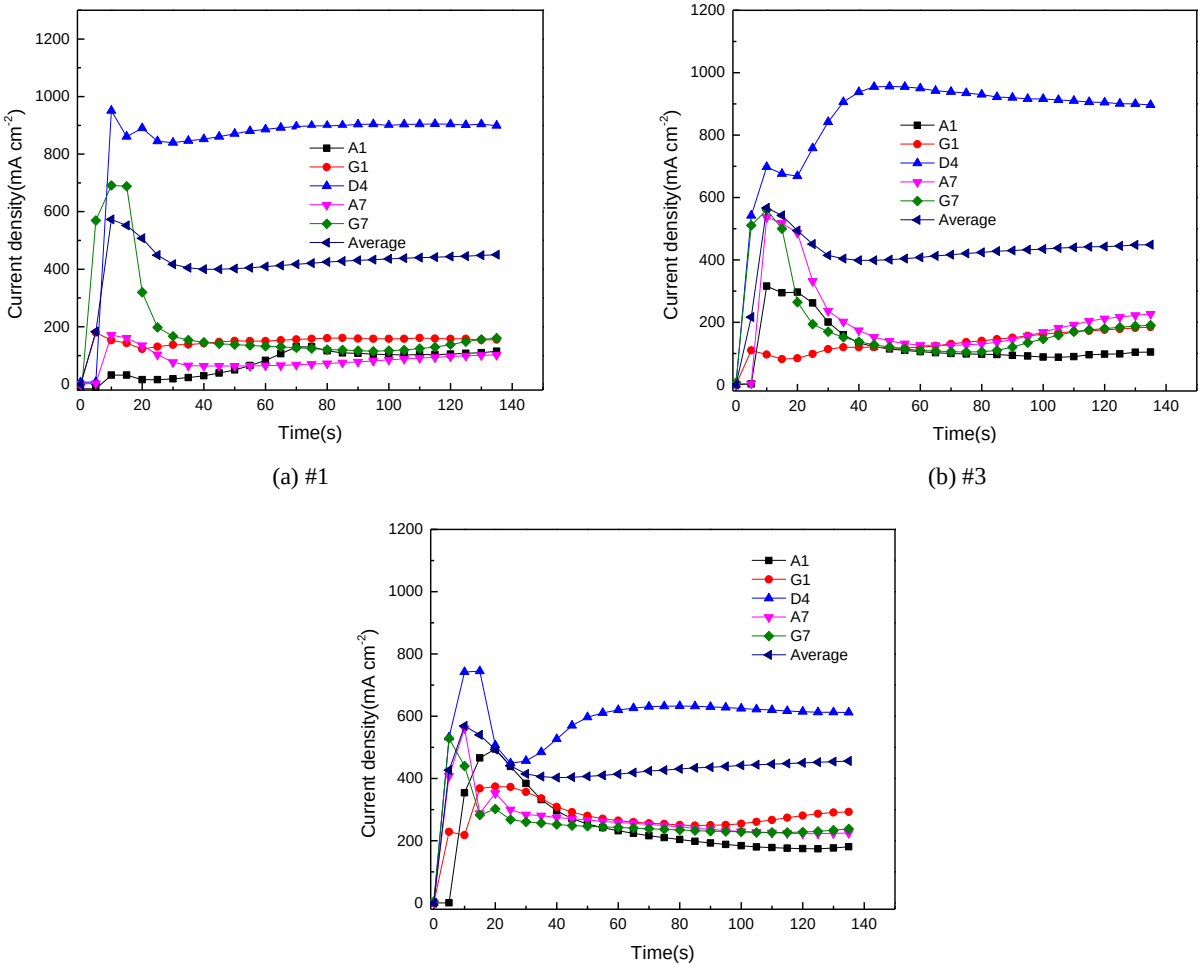

(a) #1

(b) #3

(c) #5

Fig. 6. Current density response of the single cell different zones of the single cells (#1, #3 and #5) during successful cold start at -15 °C

3.2.3. Evolution of the current density distribution of the stack during failed cold start process

Fig. 7 shows the evolution of the current density of the single cells (#1, #3 and #5) for failed cold start from -20°C at 0.5V. It shows the inconsistency in current density variation in the different cells and different regions of the same cell. The current density appeared firstly near the inlet region(G7), and then diffused to the middle and outlet regions, which was the same as the successful cold start process. It took 50s ,50s and 80s for the middle regions of the #1, #3 and #5 single cells to reach maximum current density. However, with the reaction going on, the relatively high current density at the inlet and the middle region at -20 °C results in water accumulation and freezing in the catalytic layer. Due to the difficulty of realizing hydrothermal balance, the current density in the middle region of each single cell began to decay obviously at 500s. The reverse current even appeared in the middle region of the #1 single cell. Local reversal phenomenon caused carbon corrosion[7]. The heat generated by the local reversal phenomenon contributed to rise the stack temperature. The reversal phenomenon was analyzed

in detail at 3.3.2 section. The #1, #3 and #5 single cells were completely frozen at 1935s, 2030s and 1965s, respectively. The #3 single cell had the best uniformity and longest survival time.

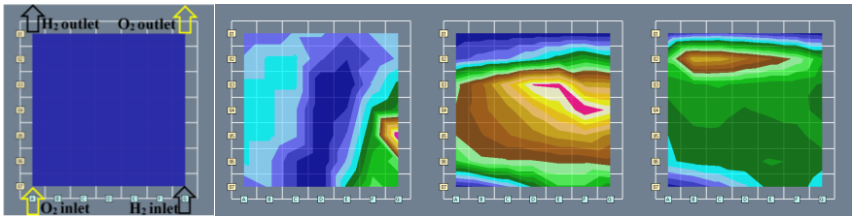

#1 0s(-20℃) 5s(-19.7℃) 50s(-16.3℃) 150s(-16.4℃)

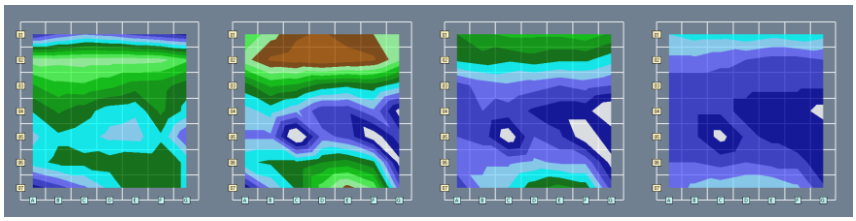

300s(-16.5℃) 500s(-16.6℃) 1750s(-17.3℃) 2250s(-17.6℃)

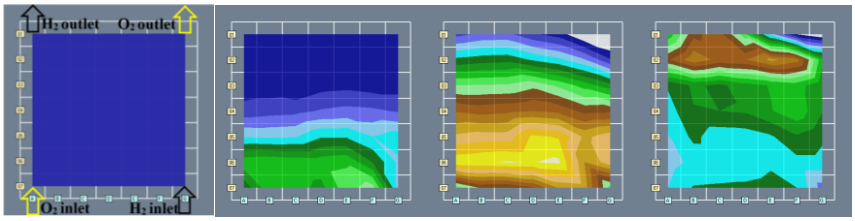

#3 0s(-20℃) 5s(-19.5℃) 50s(-15.7℃) 150s(-15.6℃)

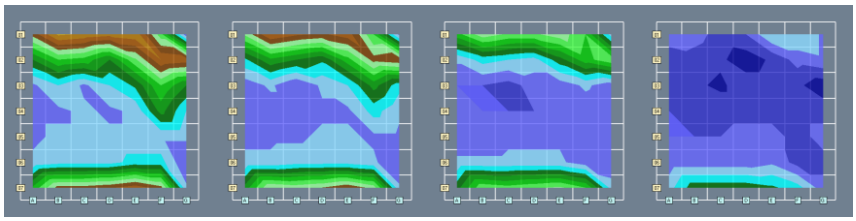

300s(-16℃) 500s(-16.1℃) 1750s(-17.1℃) 2250s(-17.3℃)

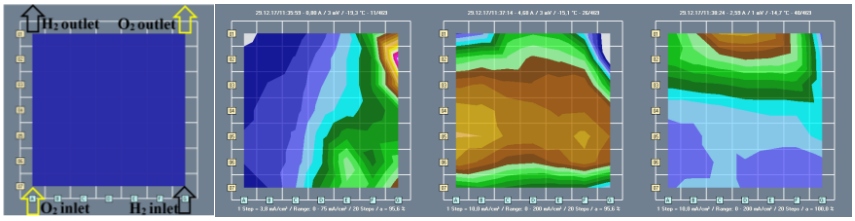

#5 0s(-20℃) 5s(-19.7℃) 80s(-15.9℃) 150s(-16.0℃)

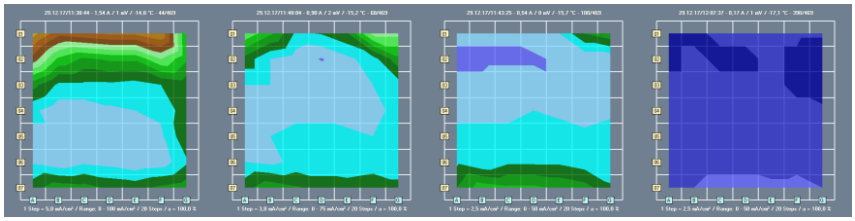

300s(-16℃) 500s(-16.1℃) 1750s(-17.2℃) 2250s(-17.4℃)

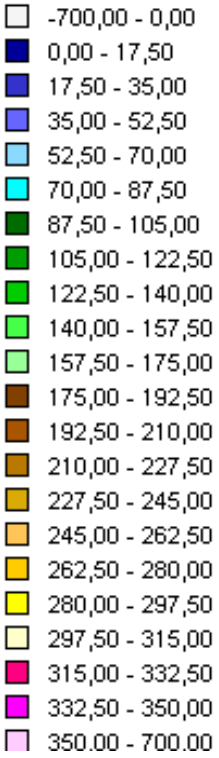

Fig. 7. Evolution of current density distribution of the single cells (#1, #3 and #5) for the failed cold start from -20°C at 0.5V

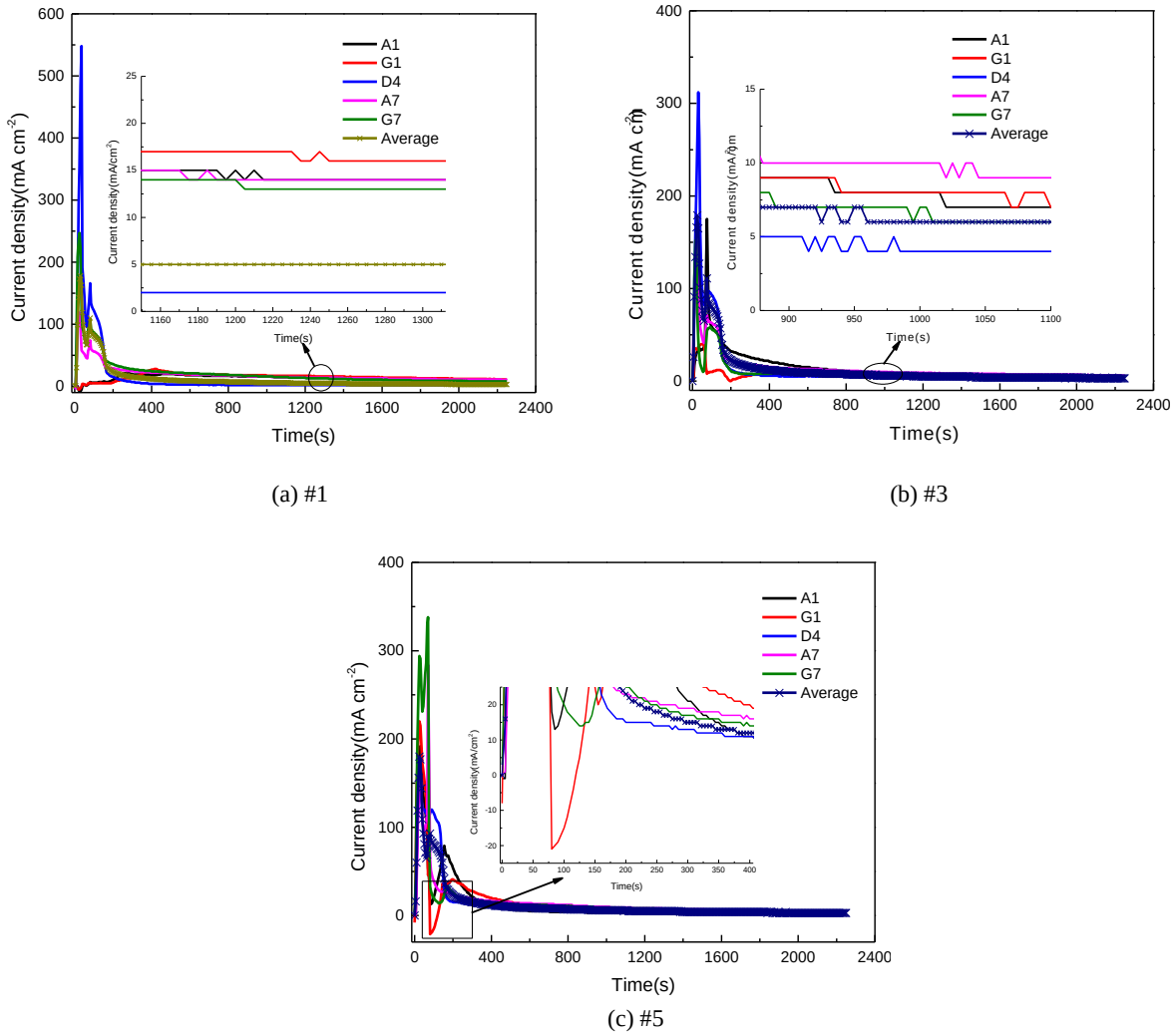

(a) #1

(b) #3

(c) #5

Fig. 8. Current density response of single cell different regions of the single cells (#1, #3 and #5) for failed cold start from -20 °C at 0.5V

Fig. 8 shows the current density response of the single cells (#1, #3 and #5) inlet, middle and outlet regions when cold start from -20°C at 0.5V. The results show that the regions near the inlet G7 and the middle D4 were still the core regions during the failed cold start at -20°C. The heat production of the stack was limited due to the low temperature. Finally, the current density of the regions near the G7 and D4 became 0 A cm^{-2} gradually because the catalyst layer and gases supply were completely blocked. Cold start performance of the stack could improve by increasing the inlet flow and ice storage capacity of porous materials.

3.3. Performance degradation

The cold start might lead to performance degradation. The main cause of the degradation was damage to the key components, such as the membrane and catalyst layer, due to water freezing[26]. However, the degradation

characteristics of the stack cold start were less involved in the literature. In this paper, the degradation mechanism of the stack cold start was analyzed by the polarization curve and monomer voltage fluctuation rate.

3.3.1. Polarization curve of the stack

The polarization curves before and after the cold start of the stack at -5°C, -10°C, -15°C and -20°C were measured as shown in Fig. 9. There was no obvious degradation in the polarization curve of the stack during the successful cold start[19]. However, the overall performance of the stack decreased obviously during the failed cold start.

After the cold start from -15°C at 2.0V, the output voltage at 1200 mA cm^{-2} current density decreased to 1.119V (the initial value was 1.64V). Moreover, the current density at the maximum power point of the stack decreased from 1000 mA cm^{-2} to 800 mA cm^{-2}. In addition, the performance degradation of the stack became more obvious after the cold start at -20°C. When the current density was only loaded into 800 mA cm^{-2}, the output voltage of the single cell was lower than 0.3 V. The maximum power also decreased. The reason was that the frost heaving stress caused by water freezing might destroy the key components of the stack, such as destroying the pore structure of the gas diffusion layer, causing the Pt particles to fall off on the catalyst, increasing in electric resistance and so on[44,45]. We could reduce the start-up voltage to increase the heat production of the stack, thereby reducing the performance damage caused by the cold start process to the stack. [19,29].

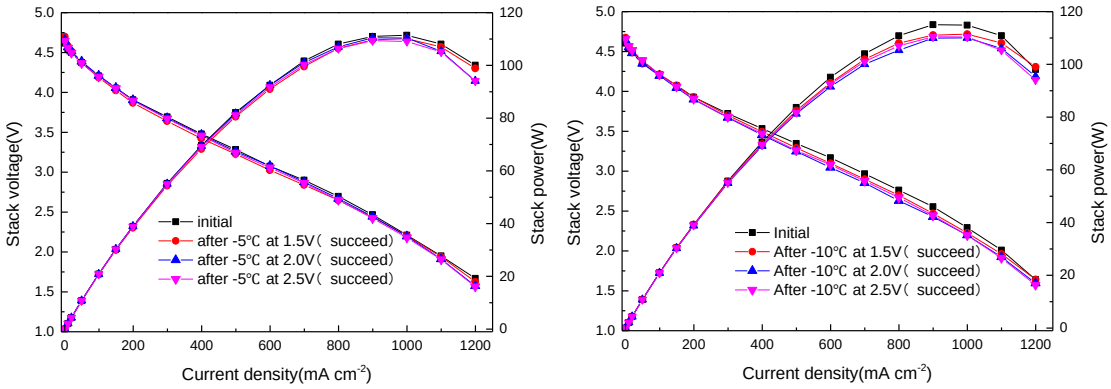

(a) Cold start from -5°C

(b) Cold start from -10°C

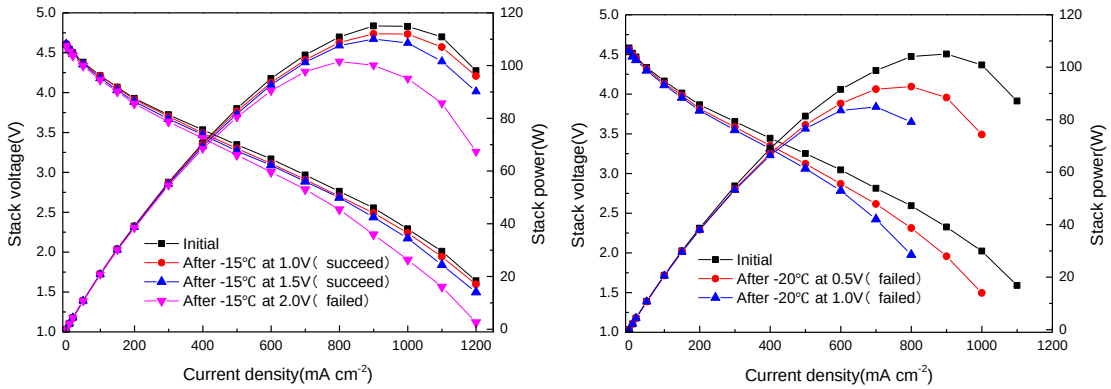

(c) Cold start from -15°C (d) Cold start from -20°C

Fig. 9. Comparison of polarization curves before and after the cold start of the stack from -5°C, -10°C, -15°C and -20°C in the constant voltage mode

3.3.2. Voltage consistency analysis

In this paper, monomer voltage fluctuation rate was used to evaluate the stack consistency.

$$C_v = \sqrt{\frac{\sum_{i=1}^{N}(\frac{V_i - \overline{V}}{\overline{V}})^2}{N}} \times 100 \qquad (2)$$

In formula (2), N is the number of single cells in the stack, $V_i (i = 1,2,3,\cdots\cdots,N)$ is the voltage of each cell, $\overline{V}$ is the average voltage of the cell.

Fig. 10 shows the results of the monomer voltage consistency analysis after cold start from -5°C, 10°C, -15°C and -20°C in constant voltage mode. The voltage consistency degradation during successful cold start was small. Even under the heavy current load (60A), the monomer voltage fluctuation rate was still about 5%, and the overall fluctuation was small. However, the voltage consistency decay was more serious with the increase of start-up voltage during failed cold start. After cold start from -20°C at 1.0V, the monomer voltage fluctuation rate reached 27.14% when the current load was only 40A. The attenuation of the monomer voltage consistency directly restricted the overall performance of the stack[46].

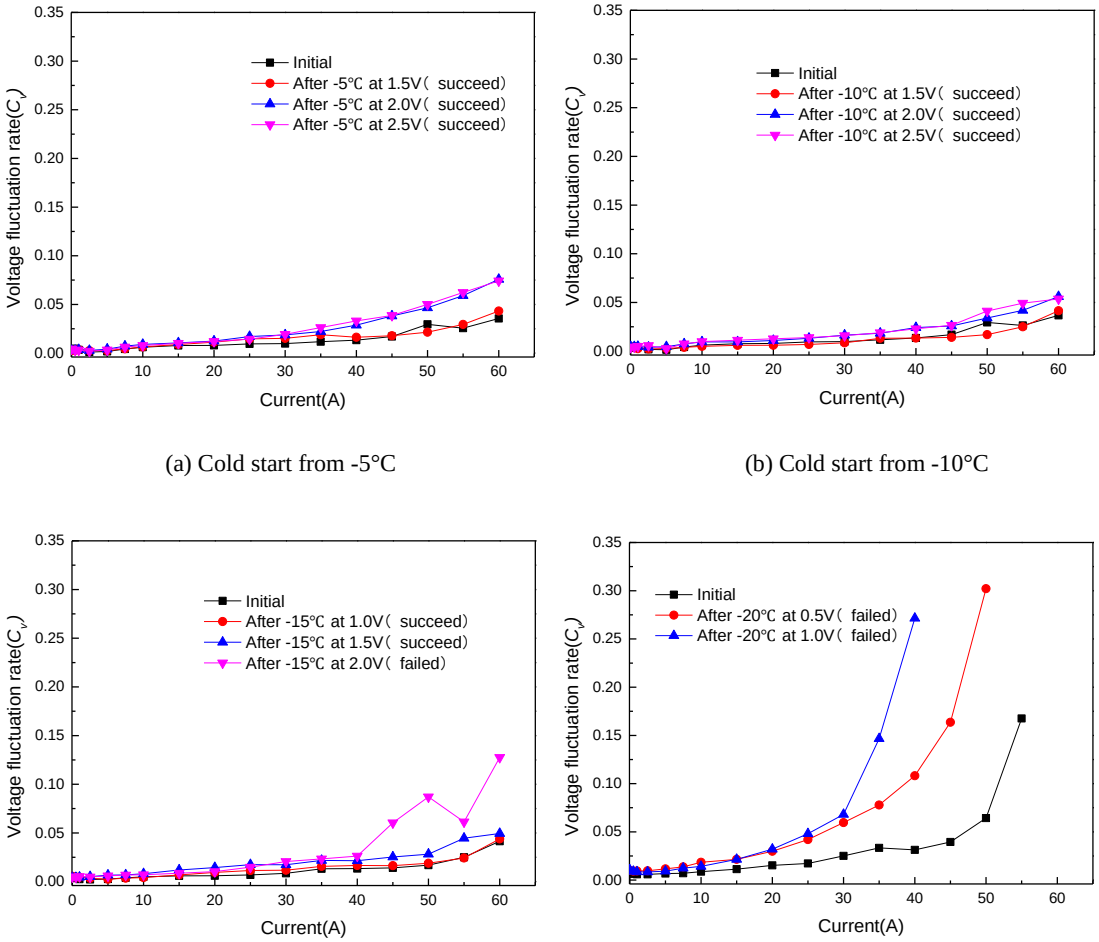

Fig. 10. Variation of voltage consistency after the cold start from -5°C, -10°C, -15°C and -20°C at constant voltage mode

Fig.11 shows the change of the polarization curves of each cell after the failed cold start. The performance degradation of the #1 single cell was more serious after the failed cold start. The performance degradation gradually decreased from the #1 single cell (near the inlet) to the #5 single cell (far away from the inlet). It is supposed that the reaction gases first reached the # 1 single cell during the startup process, which was prior to the generation of current in other single cells and produced more water so that the amount of ice formation was more. Moreover, the # 1 single cell was close to the end plate so that the heat dissipation was serious. The #1 single cell was prone to local current reversal as shown in Fig. 7. The current reversal occurred when the cell could not produce the forced current density so water electrolysis and carbon corrosion took place[7,39]. The current reversal contributed to water consumption, reducing the ice formation in the cell. Moreover, the current reversal could generate more heat, which further warmed up the cell. However, the catalytic layer might destroy, the performance of the cell would decrease obviously. In addition, the inlet gases had a great disturbance to the temperature of the #1 single cell. The poor temperature characteristic led to the water freezing more easily

occurring and therefore the damage to the key structure of the #1 cell was the most serious by frost heave stress[27]. Therefore, the performance degradation was more serious after a repeated cold start.

The stack consistency was poor after failed cold start. The performance of the # 1 single cell in the stack degraded seriously, which led to the serious attenuation of the overall performance of the stack. We could use auxiliary measures to improve the # 1 single cell cold start performance for the real applications. For example, external heat source heating and heating reaction gas, etc. Auxiliary measures could increase the consistency and durability of the stack. Compared with the auxiliary measures for the entire stack, only the auxiliary measures for the #1 single cell could reduce the complexity of the auxiliary system and the supply of external energy. It was helpful to meet the DOE standard. In addition, improve the cold start performance of single cells at the middle position and gases inlet position, the consistency and cold start performance of the stack can be improved effectively.

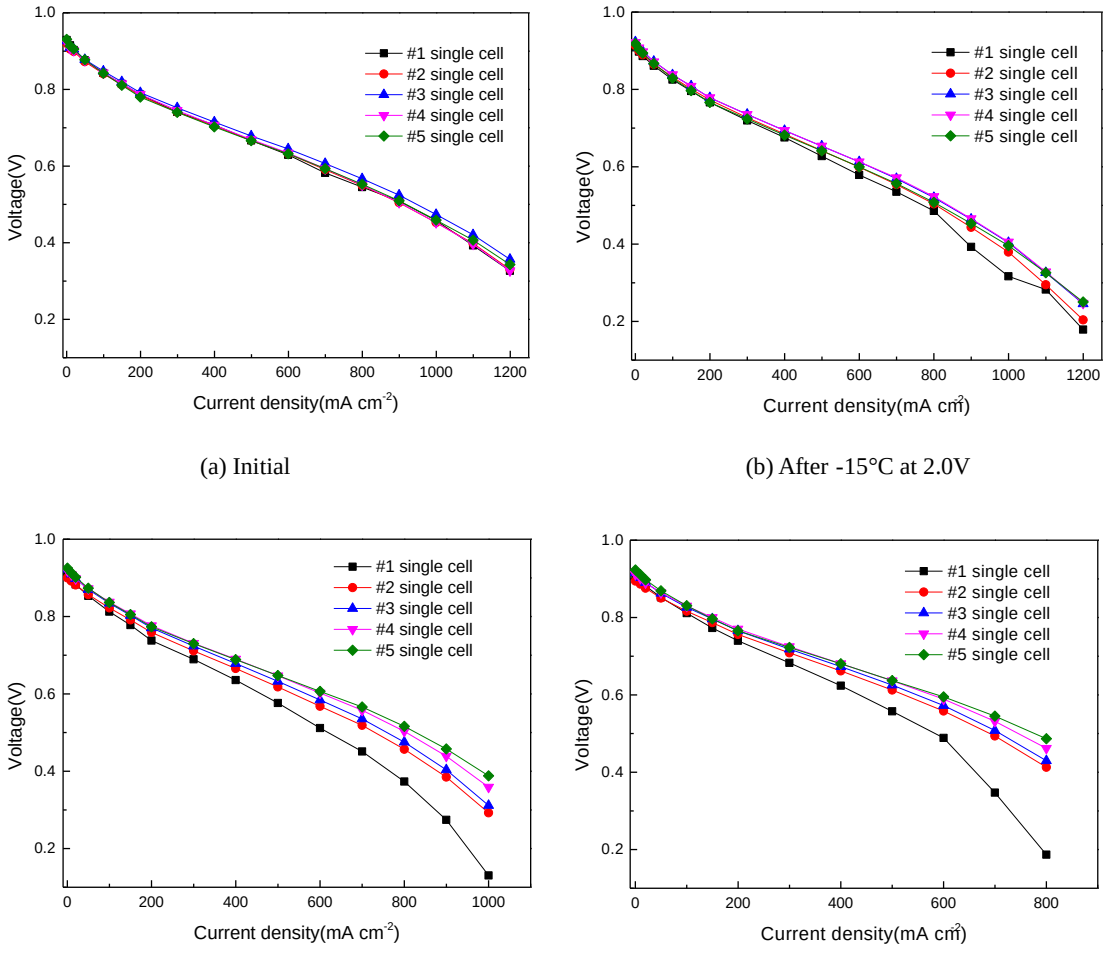

(a) Initial

(b) After -15°C at 2.0V

(c) After -20°C at 0.5V

(d) After -20°C at 1.0V

Fig. 11. The change of the polarization curves of each cell after the failed cold start (-15°C at 2.0V , -20°C at 0.5V and 1.0V)

4. Conclusions

This paper investigated the cold start characteristic of the stack in constant voltage startup mode. The evolution of the temperature and current density distribution at different regions in the constant voltage mode of the stack were investigated by the segmented technology. Finally, the performance degradation of the stack after cold start was explored through the polarization curve and the voltage consistency. This paper obtained the general rule of the stack cold start and might provide direction for the optimization cold start strategy for the real applications. This paper was an important supplement to the current published cold start studies in the literature.

1. Reducing startup voltage could improve the cold start performance of the stack and realize rapid start. The cold start capacity of the stack was good at -5°C and -10°C, and could realize rapidly cold start in 95s from -15°C at 1.0 V.
2. The cold start performance of the cell located in the middle position was obviously better than that of the cell on both sides.
3. Current density changes during cold start process of different single cells and in different areas of the same single cell were inconsistent. The #1 single cell had the best distribution uniformity because of the sufficient gases. The current density near the middle region was the highest, which played a leading role in the temperature rise of the stack. Sometimes, the local current reversal would happen. In the case of insufficient gas supplied, the gas back flow would occur.
4. The performance degradation gradually decreased from the single cell near the inlet to the single cell far away from the inlet. In the real applications, add appropriate auxiliary measures to the #1 single cell (near the inlet) and improve the cold start performance of the single cells at the middle position and gases inlet position to improve stack performance consistency.

5. Acknowledgements

The authors gratefully acknowledge the financial support from National Key Research and Development Program of China (No. 2016YFB0101319) and National Natural Science Foundation of China (No. 21776222).

6. References

[1] Ling CY, Cao H, Chen Y, Han M, Birgersson E. Compact open cathode feed system for PEMFCs. Appl Energy 2016;164:670–5. doi:10.1016/j.apenergy.2015.12.012.

[2] Jannelli E, Minutillo M, Perna A. Analyzing microcogeneration systems based on LT-PEMFC and HT-PEMFC by energy balances. Appl Energy 2013;108:82–91. doi:10.1016/j.apenergy.2013.02.067.

[3] Li W, Zhang Q, Wang C, Yan X, Shen S, Xia G, Shen S, Xia G, Zhu F, Zhang J. Experimental and numerical

analysis of a three-dimensional flow field for PEMFCs. Appl Energy 2017;195:278–88. doi:10.1016/j.apenergy.2017.03.008.

[4] Zhou Y, Luo Y, Yu S, Jiao K. Modeling of cold start processes and performance optimization for proton exchange membrane fuel cell stacks. J Power Sources 2014;247:738–48. doi:10.1016/j.jpowsour.2013.09.023.

[5] Mao L, Wang C-Y. Analysis of Cold Start in Polymer Electrolyte Fuel Cells. J Electrochem Soc 2007;154:B139. doi:10.1149/1.2402123.

[6] Li Y, Pei P, Wu Z, Ren P, Jia X, Chen D. Approaches to avoid fl ooding in association with pressure drop in proton exchange membrane fuel cells. Appl Energy 2018;224:42–51. doi:10.1016/j.apenergy.2018.04.071.

[7] Xie X, Wang R, Jiao K, Zhang G, Zhou J, Du Q. Investigation of the effect of micro-porous layer on PEM fuel cell cold start operation. Renew Energy 2018;117:125–34. doi:10.1016/j.renene.2017.10.039.

[8] Yang Z, Du Q, Huo S, Jiao K. ScienceDirect Effect of membrane electrode assembly design on the cold start process of proton exchange membrane fuel cells. Int J Hydrogen Energy 2017;42:25372–87. doi:10.1016/j.ijhydene.2017.08.106.

[9] Xie X, Zhang G, Zhou J, Jiao K. ScienceDirect Experimental and theoretical analysis of ionomer / carbon ratio effect on PEM fuel cell cold start operation. Int J Hydrogen Energy 2017;42:12521–30. doi:10.1016/j.ijhydene.2017.02.183.

[10] Huo S, Jiao K, Wan J. On the water transport behavior and phase transition mechanisms in cold start operation of PEM fuel cell. Appl Energy 2019;233–234:776–88. doi:10.1016/j.apenergy.2018.10.068.

[11] Ko J, Ju H. Comparison of numerical simulation results and experimental data during cold-start of polymer electrolyte fuel cells. Appl Energy 2012;94:364–74. doi:10.1016/j.apenergy.2012.02.007.

[12] Huo S, James N, Lee T, Wan J, Jiao K. Experimental investigation on PEM fuel cell cold start behavior containing porous metal foam as cathode flow distributor. Appl Energy 2017;203:101–14. doi:10.1016/j.apenergy.2017.06.028.

[13] Song K, Kim H. Effect of air purging and dry operation on durability of PEMFC under freeze / thaw cycles. Int J Hydrogen Energy 2011;36:12417–26. doi:10.1016/j.ijhydene.2011.06.095.

[14] Chang Y, Qin Y, Yin Y, Zhang J, Li X. Humidi fi cation strategy for polymer electrolyte membrane fuel cells – A review. Appl Energy 2018;230:643–62. doi:10.1016/j.apenergy.2018.08.125.

[15] Knorr F, Garcia D, Schirmer J, Gazdzicki P, Friedrich KA. Methanol as antifreeze agent for cold start of automotive polymer electrolyte membrane fuel cells. Appl Energy 2019;238:1–10. doi:10.1016/j.apenergy.2019.01.036.

[16] Tang H, Santamaria AD, Bachman J, Park JW. Vacuum-assisted drying of polymer electrolyte membrane fuel cell. Appl Energy 2013;107:264–70. doi:10.1016/j.apenergy.2013.01.053.

[17] Hishinuma Y, Chikahisa T, Kagami F, Ogawa T. The design and performance of a PEFC at a temperature below freezing. Jsme Int J Ser B-Fluids Therm Eng 2004;47:235–41. doi:Doi 10.1299/Jsmeb.47.235.

[18] Luo Y, Jiao K, Jia B. International Journal of Heat and Mass Transfer Elucidating the constant power , current and voltage cold start modes of proton exchange membrane fuel cell. Int J Heat Mass Transf 2014;77:489–500. doi:10.1016/j.ijheatmasstransfer.2014.05.050.

[19] Lin R, Ren YS, Lin XW, Jiang ZH, Yang Z, Chang YT. Investigation of the internal behavior in segmented PEMFCs of different fl ow fi elds during cold start process. Energy 2017;123:367–77. doi:10.1016/j.energy.2017.01.138.

[20] Amamou A, Kandidayeni M, Boulon L, Kelouwani S. Real time adaptive e ffi cient cold start strategy for proton exchange membrane fuel cells. Appl Energy 2018;216:21–30. doi:10.1016/j.apenergy.2018.02.071.

[21] Chippar P, Ju H. Evaluating cold-start behaviors of end and intermediate cells in a polymer electrolyte fuel cell (PEFC) stack. Solid State Ionics 2012;225:85–91. doi:10.1016/j.ssi.2012.02.038.

[22] Luo Y, Guo Q, Du Q, Yin Y, Jiao K. Analysis of cold start processes in proton exchange membrane fuel cell stacks. J Power Sources 2013;224:99–114. doi:10.1016/j.jpowsour.2012.09.089.

[23] Wan Z, Chang H, Shu S, Wang Y, Tang H. A Review on Cold Start of Proton Exchange Membrane Fuel Cells 2014. doi:10.3390/en7053179.

[24] Tang T, Heinke S, Tegethoff W. ScienceDirect A spatially resolved fuel cell stack model with gas e liquid slip phenomena for cold start simulations 2017;2. doi:10.1016/j.ijhydene.2017.03.236.

[25] Zhan Z, Yuan C, Hu Z, Wang H, Sui PC, Djilali N. Experimental study on different preheating methods for the cold-start of PEMFC stacks. Energy 2018;162:1029–40. doi:10.1016/j.energy.2018.08.003.

[26] Luo Y, Jiao K. Cold start of proton exchange membrane fuel cell. Prog Energy Combust Sci 2018;64:29–61. doi:10.1016/j.pecs.2017.10.003.

[27] Park G, Lim S, Park J, Yim S, Park S, Yang T, Yoon Y, Kim C. Analysis on the freeze / thaw cycled polymer electrolyte fuel cells. Curr Appl Phys 2010;10:S62–5. doi:10.1016/j.cap.2009.11.043.

[28] Alink R, Gerteisen D, Oszcipok M. Degradation effects in polymer electrolyte membrane fuel cell stacks by sub-zero operation — An in situ and ex situ analysis 2008;182:175–87. doi:10.1016/j.jpowsour.2008.03.074.

[29] Lin R, Weng Y, Lin X, Xiong F. ScienceDirect Rapid cold start of proton exchange membrane fuel cells by the printed circuit board technology. Int J Hydrogen Energy 2014;39:18369–78.

doi:10.1016/j.ijhydene.2014.09.065.

[30] Lin R, Lin X, Weng Y, Ren Y. Evolution of thermal drifting during and after cold start of proton exchange membrane fuel cell by segmented cell technology. Int J Hydrogen Energy 2015;40:7370–81. doi:10.1016/j.ijhydene.2015.04.045.

[31] Kim SG, Kim MJ, Sohn YJ. Segmented cell approach for studying uniformity of current distribution in polymer electrolyte fuel cell operation. Int J Hydrogen Energy 2015;40:11676–85. doi:10.1016/j.ijhydene.2015.05.055.

[32] Lin R, Weng Y, Li Y, Lin X, Xu S. ScienceDirect Internal behavior of segmented fuel cell during cold start 2014;9:0–10. doi:10.1016/j.ijhydene.2013.12.083.

[33] Ishikawa Y, Hamada H, Uehara M, Shiozawa M. Super-cooled water behavior inside polymer electrolyte fuel cell cross-section below freezing temperature 2008;179:547–52. doi:10.1016/j.jpowsour.2008.01.031.

[34] Jiao K, Alaefour IE, Karimi G, Li X. Cold start characteristics of proton exchange membrane fuel cells. Int J Hydrogen Energy 2011;36:11832–45. doi:10.1016/j.ijhydene.2011.05.101.

[35] Jiao K, Li X. Effects of various operating and initial conditions on cold start performance of polymer electrolyte membrane fuel cells. Int J Hydrogen Energy 2009;34:8171–84. doi:10.1016/j.ijhydene.2009.07.102.

[36] Khandelwal M, Lee S, Mench MM. One-dimensional thermal model of cold-start in a polymer electrolyte fuel cell stack. J Power Sources 2007;172:816–30. doi:10.1016/j.jpowsour.2007.05.028.

[37] Jiao K, Li X. Cold start analysis of polymer electrolyte membrane fuel cells. Int J Hydrogen Energy 2010;35:5077–94. doi:10.1016/j.ijhydene.2009.09.004.

[38] Chen H, Xu S, Pei P, Qu B. ScienceDirect Mechanism analysis of starvation in PEMFC based on external characteristics. Int J Hydrogen Energy 2018:1–10. doi:10.1016/j.ijhydene.2018.11.135.

[39] Zhong D, Lin R, Liu D, Cai X. Structure optimization of anode parallel fl ow fi eld for local starvation of proton exchange membrane fuel cell. J Power Sources 2018;403:1–10. doi:10.1016/j.jpowsour.2018.09.067.

[40] Kang J, Won D, Park S, Lee J, Ko J, Kim J. Accelerated test analysis of reversal potential caused by fuel starvation during PEMFCs operation. Int J Hydrogen Energy 2010;35:3727–35. doi:10.1016/j.ijhydene.2010.01.071.

[41] Oszcipok M, Zedda M, Riemann D, Geckeler D. Low temperature operation and influence parameters on the cold start ability of portable PEMFCs 2006;154:404–11. doi:10.1016/j.jpowsour.2005.10.035.

[42] Cui X. Experimental study of variable operating parameters effects on overall PEMFC performance and spatial performance distribution 2016;115:550–60. doi:10.1016/j.energy.2016.08.086.

[43] Jiao K, Alaefour IE, Karimi G, Li X. Simultaneous measurement of current and temperature distributions in a

proton exchange membrane fuel cell during cold start processes. Electrochim Acta 2011;56:2967–82. doi:10.1016/j.electacta.2011.01.019.

[44] Mehta V, Cooper JS. Review and analysis of PEM fuel cell design and manufacturing 2003;114.

[45] Yan Q, Toghiani H, Lee Y, Liang K, Causey H. Effect of sub-freezing temperatures on a PEM fuel cell performance , startup and fuel cell components 2006;160:1242–50. doi:10.1016/j.jpowsour.2006.02.075.

[46] Li Y, Zhao X, Liu Z, Li Y, Chen W, Li Q. ScienceDirect Experimental study on the voltage uniformity for dynamic loading of a PEM fuel cell stack 2015;0:3–11. doi:10.1016/j.ijhydene.2015.04.058.